Nanomechanical characterization of bone quality depending on tissue age via advanced bi-modal Atomic Force Microscopy

An Undergraduate Honors Thesis
Submitted to the Department of Mechanical Engineering
The Ohio State University
In Partial Fulfillment of the Requirements
For Graduation with Honors Distinction in Mechanical Engineering

Ran Zhuang
November 2019

Advisor: Hanna Cho, Ph.D.

Abstract

As an engineering view, bone is a smart material whose structure and material properties can be controlled in response to the external loading to support and protect inner organs of the body. To achieve this, bone actively remodels its shape and material composition by removing old bone part and replacing it with new bone, which results in hierarchical structure and heterogeneity of bone. Even though the bone mineralization process plays a key role to modulate functional demands of bone, the underlying mechanism have not fully understood yet. In order to understand the mechanism, it is essential to examine bone quality depending on its tissue age. Moreover, due to its hierarchical structure, investigating it in a variety of scales are needed. Although the morphology and mechanical property of bone has been studied in a various scale, scrutinizing them together in its fibrillar scale has not been widely conducted. In this study, we used mandibular bone planted dental implant because the tissue age can be easily determined by the distance from the implant. We investigated the chronical changes of morphology and mechanical property in a fibrillar scale depending on the tissue age by employing bi-modal AFM technique. Finally, we successfully obtained topographic and its mechanical stiffness maps of the sample, which indicated that the old bone matrix showed more organized structure and higher stiffness when compared with the new bone matrix.

Acknowledgments

I would like to thank my research advisor, Dr. Hanna Cho. Dr. Cho provided me an opportunity to get involved in her research project in her course System Dynamics and Vibration class. After talking with Dr. Cho about my future master's degree plan, she introduced the research direction to me, and I gloriously got the research program opportunity. Dr. Cho gave me advice not only in the research area but also in my whole study life. During the meetings with Dr. Cho, I learned many things other than the research program, including how to manage study time and the relationship with professors.

I would also like to thank my friend, Jinha Kwon, for his patient and continual help as a constant mentor. He is not only my mentor but also my friend, who I could share interesting ideas in both research and life. I received so much help from Jinha. He taught me how to use all kinds of devices for my research and help me a lot in revising my thesis. I appreciate all the time and efforts you spent on me. And I hope you could successfully finish your Ph.D. degree.

Contents

Abstract....3
Acknowledgments....4
List of figures....6
Chapter 1. Introduction....7
1.1 Bone....7
1.2 Objective of the study....8
1.3 Significance of the study....9
1.4 Overview of thesis:....9
Chapter 2. Background....10
2.1 Bone information....10
2.1.1 Level II: structural components....11
2.1.2 Level III: Fibril ordered array....11
2.2 Bone quality determination....12
2.2.1 Mineral phase....12
2.2.2 Collagen....12
2.3 Remodeling process....13
Chapter 3: Methodology....15
3.1 Sample preparation....15
3.2 AFM introduction – Contact mode....16
3.3 Bi-modal AFM....18
3.4 Calibration....20
3.4.1 Spring Constant....20
3.4.2 Tune....21
3.4.3 Elasticity calculate parameter....22
Chapter 4: Results and Discussion....24
Chapter 5: Conclusion....30
5.1 Summary....30
5.2 Future work....30
References....31

List of figures

Figure 1. Scheme showing the hierarchical organization of bone from the macro- to the nanoscale. Reproduced with permission.[1] Copyright 2015, Nature Publishing Group. 11

Figure 2. The interface of the implant and bone matrix separately captured by 5x objective lens (a), and 20x objective lens (b). The blue box represents the old bone and the red box represented the new bone where bi-modal AFM was performed. 16

Figure 3. Basic diagram of AC mode imaging 17

Figure 4. Tip oscillation amplitude as it approaches the surface**Error! Bookmark not defined.**

Figure 5. AM-FM Mode. The first mode amplitude is controlled to create a topographic image of the sample (blue). The second mode is used to calculate elasticity and tip-sample stiffness (red). 19

Figure 6. Thermal Data for spring 21

Figure 7. First resonant frequency of tune map 22

Figure 8. Silica Sample for finding tip radius 23

Figure 9. Optical microscopy image at the interface of the implant and bone matrix captured by 5x objective lens a), and 20x objective lens b). The red box represents the new bone area while the blue box represented the old bone area where bi-modal AFM 24

Figure 10. Nanoscale mapping of morphology and materials properties obtained by bi-modal AFM. (a), (b) shows topographic and mechanical information, respectively in old bone area. (c), (d) shows topographic and mechanical information in new bone area. 25

Figure 11. Morphology and stiffness maps of the bone in 10x10 µm2 scale obtained by bi-modal AFM. (a), (d) shows topographic information of the sample in old bone and new bone area respectively. (b), (e) means surface texture of the sample, and (c), (f) 26

Figure 12. Morphology and stiffness maps of the bone in 2x2 µm2 scale obtained by bi-modal AFM. (a), (d) shows topographic information of the sample in old bone and new bone area respectively. (b), (e) means surface texture of the sample, and (c), (f) ar 27

Figure 13. The boxplot representation of the mechanical property (Young's modulus) of new bone and old bone area obtained from 10x10 µm2, and 2x2 µm2 scanning area by bi-modal AFM respectively. 28

Figure 14. (a), (b) show the histogram representation of the Young's modulus from 10x10 µm2, and 2x2 µm2 scanning area by bi-modal AFM respectively. 29

Chapter 1. Introduction

1.1 Bone

As an engineering point of view, bone is a smart material whose properties can be changed in a controlled fashion by external stimuli. Beyond basic functions of bone such as supporting and protecting the various organs of the body, bone serves a variety of mechanical, synthetic, metabolic, and remodeling functions. To achieve this, bone is made in a sophisticated way with a highly-heterogeneous material and hierarchical structure, consisting of soft organic constituents (i.e., mostly type I collagen) and hard inorganic mineral (i.e., crystalline carbonated apatite). Bone itself is lightweight but strong, and it optimizes the structure and material in response to functional demands of the mechanical loading during the entire lifespan by remodeling itself. During the remodeling process, mature bone tissues are removed by osteoclasts (i.e., bone breaking cells), then the collagen molecules are secreted by osteoblasts (i.e., bone forming cells) to build structural matrix and fill the removed structure. This soft structural matrix is strengthened by the subsequent mineral deposition. Thus, the mineralization during the bone remodeling process plays a key role in modulating structural and compositional heterogeneity of bone, often referred as *bone quality*, and finally controlling mechanical property. To clarify its underlying mechanism, characterizing the bone quality in a same length scale as collagen fibril and carbonated apatite is essential. Although Scanning Electron Microscopy (SEM) and Transmission Electron Microscopy (TEM) has been widely used to study nanoscale structure of bone,

these techniques only provide nanoscale morphological information of a sample and require specific preparation such as electrical coating on the sample. On the other hand, the nanoindentation technique that uses small tip to indent onto a sample also has been widely used to measure mechanical properties of the sample. However, Nanoindentation only provides point information of a sample and the size of indented point is too large to distinguish collagen and mineral on the bone sample. Thus, it cannot provide heterogeneity information of the sample. To overcome these limitations, we applied an advanced Atomic Force Microscopy (AFM) technique, called bi-modal AFM. This tool provides topographic information and mechanical property of the sample simultaneously in nanometer scale by utilizing two resonance frequencies. In this study, we successfully characterized the chronical change of bone quality in a planted dental implant sample with 4 weeks of healing period, in which age of the bone tissue can be easily identified by the location from the metallic implant.

1.2 Objective of the study

Objective of this study is to characterize bone quality depending on tissue age by employing bi-modal AFM technique. In this study, the sample was prepared on a glass slide and well-polished to be suitable for bi-modal AFM. we carefully calibrated the AFM system to obtain quantitative results and characterized mechanical property (i.e., young's modulus) of the sample as well as its topographic information. Finally, the mechanical property depending on the location indicating new and old bone area was analyzed to compare each other

statistically.

1.3 Significance of the study

This is the first study to characterize the bone quality depending on tissue age in nanometer scale through the bi-modal AFM technique. This study helps to gain a better understanding of heterogeneous feature of bone depending on the chronical change, which helps to expand understanding of bone healing and remodeling process. In addition, there would be two future applications of this study: engineering and medical application. For engineering application, the understanding obtained this research could be used to develop new-generation smart materials mimicking bone's behavior and features. On the other hand, it would be helpful to treat variety of medical issues by promoting bone healing and remodeling process.

1.4 Overview of thesis:

This thesis consists 5 chapters. Chapter 2 will introduce all detail information of bones related to the research. Chapter 3 will talk about the information of the device used for the experiment, the sample preparation, and experimental procedure of the research. The result obtained during the experiments will be written in Chapter 4. Finally, in Chapter 5, there will be a conclusion of how results are related to the goal and the future work of the experiment.

Chapter 2. Background

2.1 Bone information

Bone is a heterogeneous and anisotropic nanocomposite. The structure composition is shown in Figure 1 from macroscale to nanoscale. Weiner & Wagner [3] originally divided the structure of bone from nanoscale to macroscale and invented seven hierarchical levels of organization of the bone family in 1998. In their theory, all bones have a shell of compact bone, which could vary a lot depending on the bone type. Then in the shell, the trabecular bone, made of spongy bone and compact bone, fills up the inner space of the bone, in level VI. Then in level V, the cylindrical motifs of compact bone are mainly made of osteons and some Haversian canals in between. The osteons have a similar concentric lamellar structure without cement line. The cement line forms at where resorption stops. The collagen fibril array consists the osteons in level IV. It could organize different patterns based on their location. Then in level II and III, the fibril array is made of minerals and collagens. And N. Reznikov et al [3] separate the bone structure form macro scale to nanoscale into nine levels, considering the structure of bone. Similarly, he puts level II and III as fibril made of minerals and collagens.

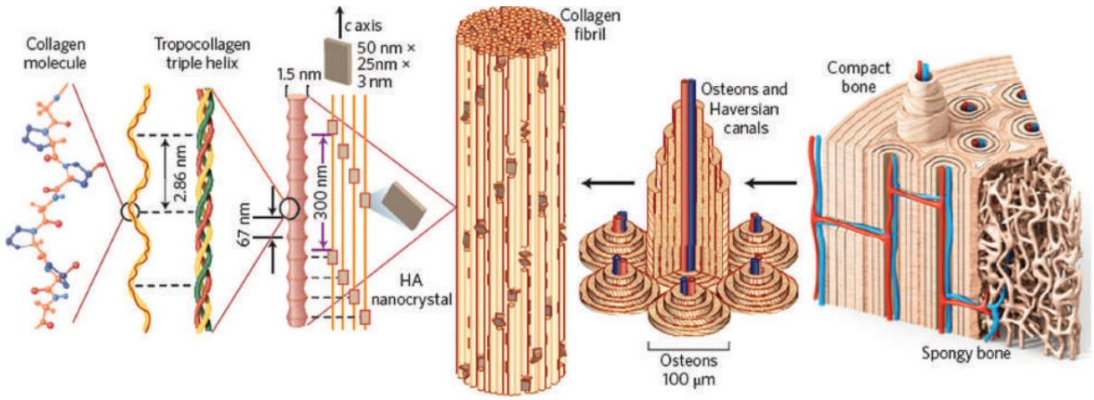

Figure 1. Scheme showing the hierarchical organization of bone from the macro- to the nanoscale. Reproduced with permission.[1] Copyright 2015, Nature Publishing Group.

2.1.1 Level II: structural components

The mineralized collagen fibrils form the second hierarchical level. The collagen is organized by fibrils with 80 – 120 nm in diameter, which could be oval shape in cross-section. The collagen grows from a disordered precursor phase within the gaps inside the fiber into an overlap zone. The final result is the mineralized collagen fibril that compromised of a layer of plate-shaped crystals.

2.1.2 Level III: Fibril ordered array

Type I collagen fibrils consist of the fibril array in level 3. They have a strong tendency of self-assemble into arrays. The assembly process starts from the endoplasmic reticulum of the osteoblasts, grows to the cytoplasm. Then finally, the type I collagen fibril extends into the extracellular space.

2.2 Bone quality determination

The level I, in N. Reznikov's theory [3] are the major components, which are the most basic materials. The material concludes the mineral carbonated hydroxyapatite, type I collagen and water, with minor amounts of other collagen types.

2.2.1 Mineral phase

Bone mineral is the inorganic component of bone tissue, which gives bones compressive strength. Mineral phase in bone has ca. 40 GPa for young's modulus, which makes bone hard but brittle. The mineral phase in nanoscale is carbonated hydroxyapatite in the form of thin plate-shaped crystals, which is 1.5 – 4 nm thick. The mature carbonated hydroxyapatite crystals are relatively disordered at atomic level because of its highly disordered precursor phase.

2.2.2 Collagen

Collagen is the main structural protein in human body. And depending on the degree of mineralization, collagen tissue behaves rigid in bone. Collagen in bone has ca. 5 GPa for young's modulus, which makes bone soft but tough. According to Yan Liu, Dan Luo, and Tie Wang 2016 [12] in their paper "Hierarchical Structures of Bone and Bioinspired Bone Tissue Engineering", the organic part of bone consists of about 90 percent of collagen and water. Type I collagen is the most abundant protein present in bone, consisted of a highly repetitive amino acid sequence. The collagen is comprised of unique triple-helical tropocollagen molecules, which are about 300 nm in length and 1.5 nm in diameter.

2.3 Remodeling process

Bone is a living organ that undergoes remodeling throughout life. Adults have only 206 bones; however, newborns have more than 270 pieces of bones. According to Hadjidakis DJ, Androulakis II 2006 in “Bone remodeling” [4], when people grow up, some bones grow together by applying the remodeling process. When a bone gets microdamage, body needs to fix this defect. The name of this recovering process is called remodeling, which is the function of osteoblasts and osteoclasts. The resorption and formation in human body are equilibrium. During this process, the old bones are replaced by new bones continuously to react to the stress and strain put on body. This phenomenon is defined by Frost in 1990, called bone remodeling in 1990 [5].

The remodeling process is executed by the cooperation of osteoclasts and osteoblasts. This collaboration forms a basic multicellular unit (BMU). The BMU has morphological difference in cortical and trabecular bone, but this difference is not biological. The BMU generates a cylindrical canal about 2000 μm long and 150~200 μm in diameter. This canal slowly crosses the bone at speed 20-40 μm per day. According to Petrtly’s research in 1996 [6], in every period, about 10 osteoclasts create a cylindrical space in the direction where force comes from. Then a few thousands of osteoblasts fill the space, remodeling bones this way by 2% to 5% of cortical bone in this way, according to Parfitt’s research in 1994 [7]. Because the trabecular bone has a larger ratio between surface area and volume compared to cortical bone, it is easier to remodel. The speed of osteoclasts when

they grow through the trabecular surface is about 25 μm per day. Finally, the Osteoclasts dig a trench with depth of 40-60 m.

The remodeling cycle consists of three consecutive phases: resorption, reversal, and formation. Firstly, resorption starts from the partially differentiated mononuclear preosteoclasts to the bone surface and form multinucleated osteoclasts. After the resorption process, a reversal process begins when mononuclear cells appear on the bone surface. These cells have two functions, preparing the surface for new osteoblasts to begin bone formation and providing signals for osteoblast differentiation and migration. The last phase is formation phase, which is followed with osteoblasts covering bone until the old bone is completely replaced by new one. Then the surface is covered with flattened lining cells. A long resting period begins and lasts until the next remodeling process starts. The period of different phase has different lengths. Resorption lasts for about 2 weeks; the reversal phase takes up to 4 or 5 weeks, while formation continues for 4 months until the new bone structural unit is completely created.

Chapter 3: Methodology

3.1 Sample preparation

In order to study the bone quality, the sample of the dog's dental implant slice was used to simulate general bone structure. The sample was prepared and provided by the College of Dentistry through a collaboration with Dr. Do-Gyoon Kim, as shown in figure 2. Following IACUC approval, an adult male beagle dog (10-15 kg) received a dental implant at the second premolar in its mandible. At the 4-weeks of post-implantation healing period, the animal was euthanized to dissect the bone implant construct. The specimen was fixed in a formalin solution for 7 days, and embedded in methyl methacrylate resin, and cut to expose bone and implant interface. Finally, the section was polished with 1 μm diamond paste and prepared on a glass slide. Figure 2 shows the optical microscopy image of a prepared sample at the interface of the implant and bone matrix.

The silver rectangle part in middle of the figure below is the implant metal. The pink area is the bone tissue of bone. When the sawtooth shape implant embedded into bone, the old bone structure were removed, and the new bone area grew from old bone to match the saw tooth edge of metal implant. Asa a result, the bone tissue in triangle part is new bone area and tissue out of triangle part is old bone area.

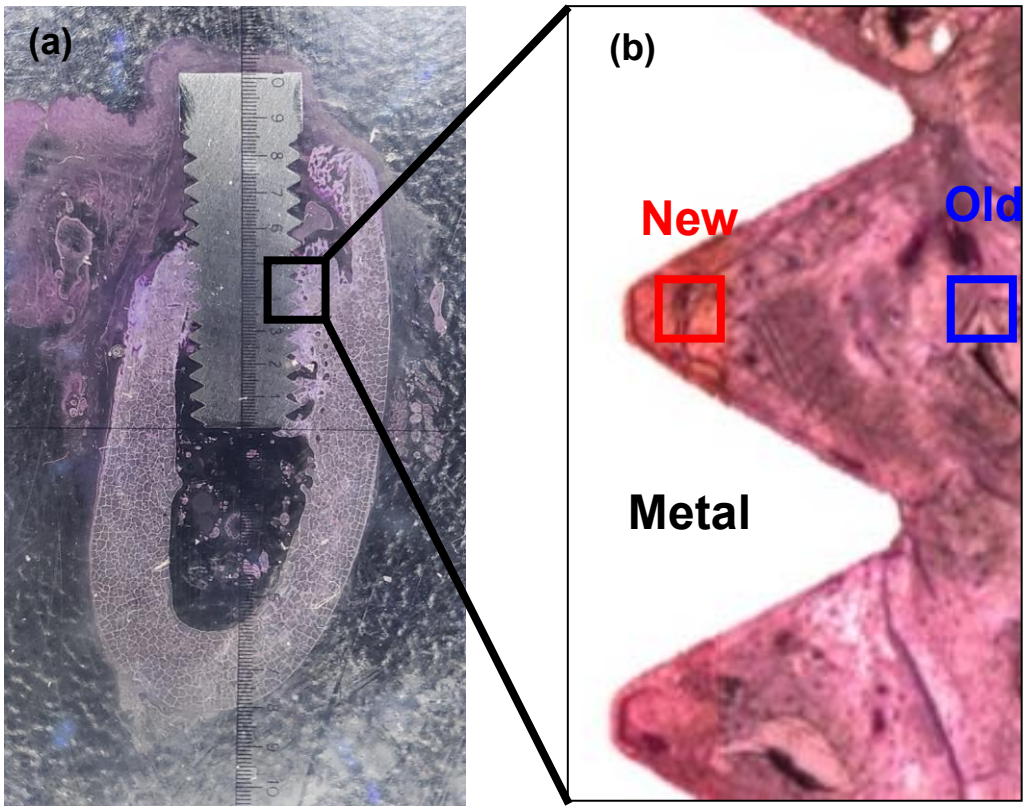

Figure 2. The interface of the implant and bone matrix separately captured by 5x objective lens (a), and 20x objective lens (b). The blue box represents the old bone and the red box represented the new bone where bi-modal AFM was performed.

3.2 AFM introduction – Contact mode

In tapping mode, the cantilever is typically oscillated mechanically by a small piezo electric actuator very near the cantilever chip. Before imaging, the drive frequency is swept over a broad range to locate the first resonance of the cantilever. Then, the drive frequency is set at or near that resonance frequency. The optical detector senses the oscillatory motion of the cantilever and the electronics inside the controller measure the amplitude of this oscillation and also the phase with respect to the drive signal. Tapping mode has a higher resolution than classic contact mode AFM because it avoids the lateral force from tip.

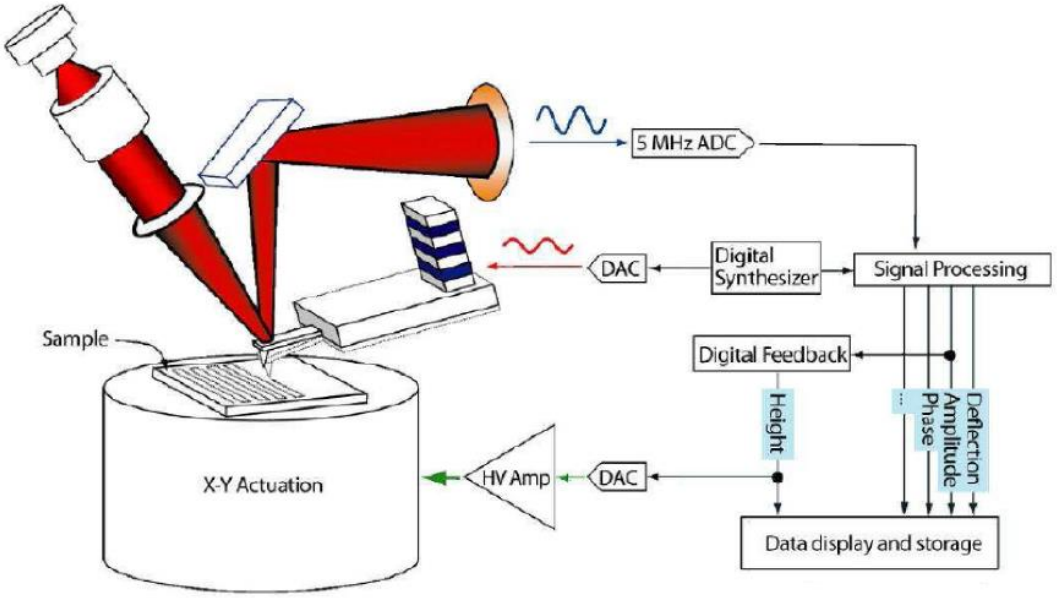

Figure 3. Basic diagram of AC mode imaging [8]

When thinking about tapping mode, it is a useful experiment to dissect a tapping mode force plot. A tapping mode force plot collects the cantilever amplitude as the oscillating tip is moved towards the surface, and away again. This is shown in figure 4. The cantilever is oscillating above a flat sample surface. In this force plot the cantilever was oscillating at resonance with an amplitude of 105 nm. That means the tip swings sinusoidally from 105 nm below the rest, to a position to 105 nm above. The amplitude remains constant until the resting position of the cantilever gets within of the oscillation is just barely touching the surface. When the cantilever closer to the surface, the tip oscillation need to be reduced. The equations of motion produce something that's very nearly a sine wave with a

reduced amplitude.

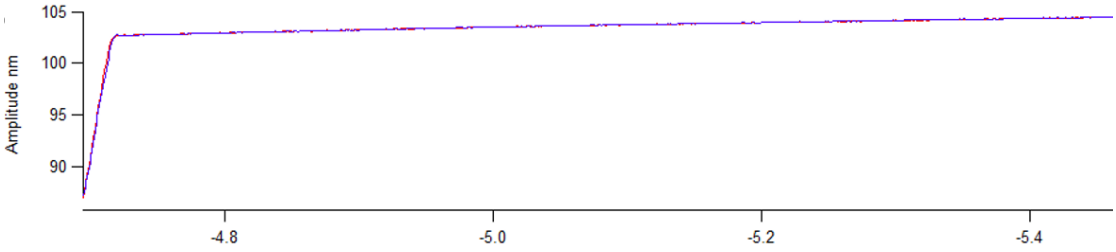

Figure 4. Tip oscillation amplitude as it approaches the surface

3.3 Bi-modal AFM

In this research we employed an advanced AFM technique, called bi-modal AFM. Bi-modal AFM imaging combines the features and benefits of normal tapping mode (also called AM) with fast scanning and quantitative, high sensitivity Frequency Modulation (FM) mode. When operating in standard AM-FM mode, there are three feedback loops. The topography, operated in normal tapping mod, feedbacks on the cantilever oscillation amplitude, providing non-invasive, high quality imaging. To accomplish second mode, drive frequency needs to be adjusted to keep the phase at 90° on resonance. This resonant frequency could sensitively measure the interaction of the tip-sample. In short, the stiffer sample is, the higher value the second resonance will be while a softer sample shifts it to a lower value. This can be converted into a quantitative modulus measurement through a variety of mechanical models. The final feedback is optional, but when enabled, maintains a constant second mode oscillation amplitude, which is used to calculate the tip-sample stiffness. This parameter is called as a drive setpoint in the software. The second mode spring constant can be calculated from this

equation:

$$K_2 = (\frac{\omega_2}{\omega_1})^2 \cdot K_1$$

As with conventional AM mode, AM-FM is a quantitative technique in which the conservative and dissipative tip-sample interactions can be separated.

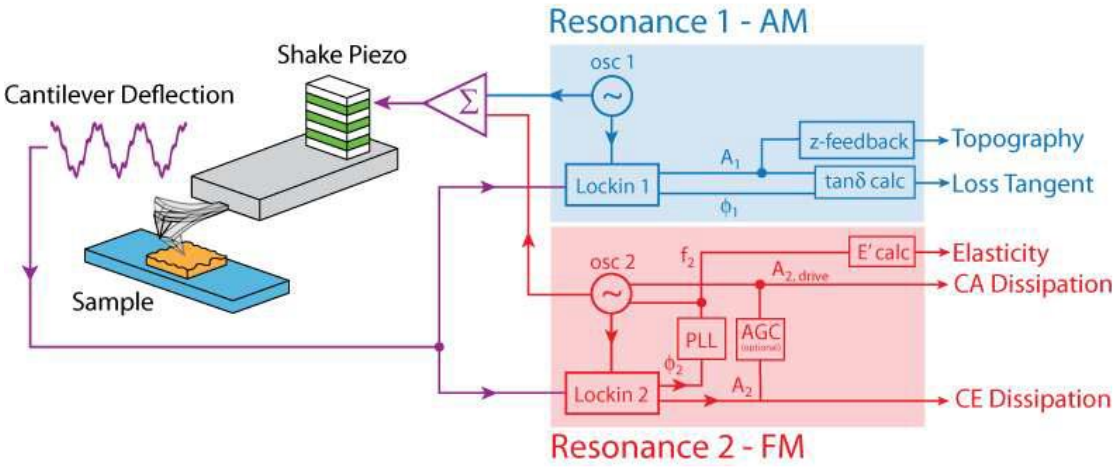

Figure 5. AM-FM Mode. The first mode amplitude is controlled to create a topographic image of the sample (blue). The second mode is used to calculate elasticity and tip-sample stiffness (red). [8]

3.4 Calibration

To setup the AFM experiment, the following parameters are needed to be calibrated. Here are the steps need calibration.

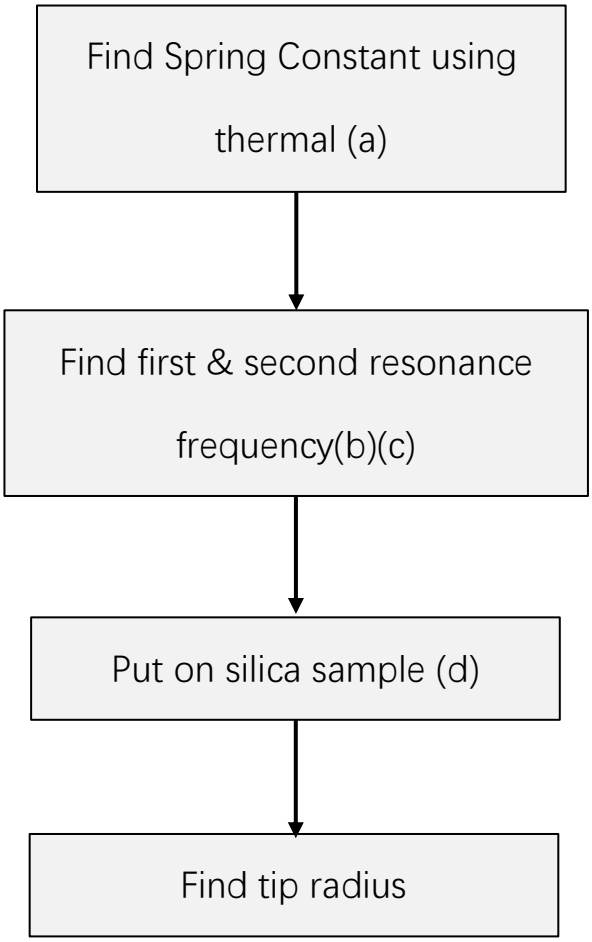

3.4.1 Spring Constant

Spring constant is the stiffness of cantilever, of which nominal value is provided by the commercial company but varies slightly by each cantilever. As such, the spring constant needs to be calibrated to obtain the force by measuring the cantilever deflection. We used a thermal method in this research. Determining the spring constant is a quick procedure, according to the SPM application manual

[8]:

1. Correct for Virtual Deflection effect in the AFM hardware.
2. Calibrate the relationship between cantilever deflection and vertical cantilever motion. The name is called InvOLS (Inversed Optical Lever Sensitivity), measured in nm/V.
3. Lastly, withdraw tip and perform a thermal to determine the cantilever's resonant frequency. The algorithm in the program computes the spring constant using the qui-partition theorem.

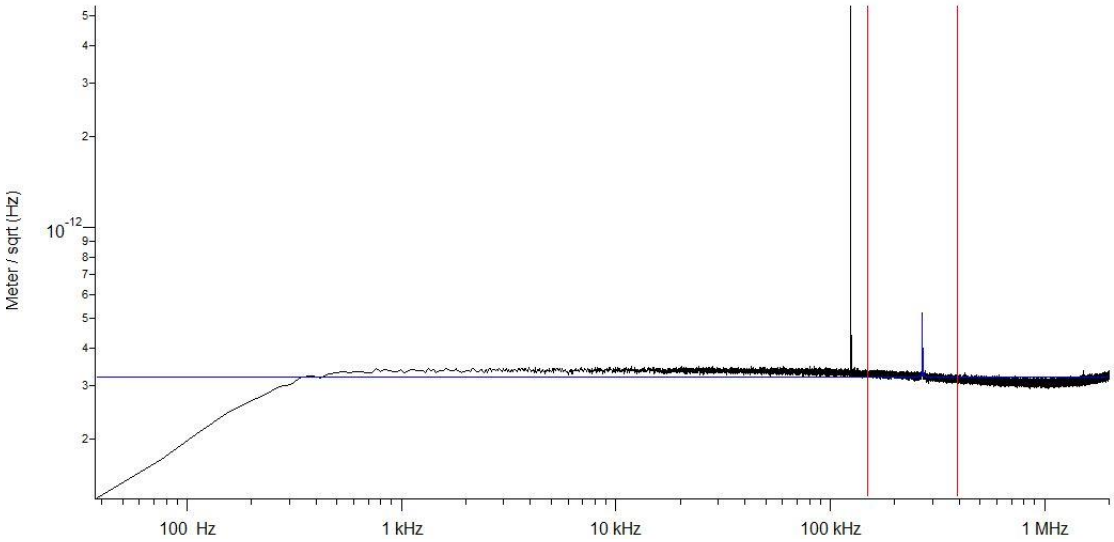

Figure 6. Thermal Data for spring

3.4.2 Tune

The tune is used to find the first and second resonances of cantilever. The steps to setup tune are as follows [8]:

1. For the cantilever AC160, setup the tune value range. The first tune is typically in the range of 200 kHz - 400 kHz; the second tune is in the range

of 1000 kHz - 2000 kHz.

2. Click the 'Auto Tune' button for the frequency sweeping to commence. The piezo shaker applies a frequency ramp through the Auto Tune from low to high frequencies. The cantilever gives the greatest oscillation amplitudes at its resonant frequencies, allowing the tune algorithm to locate them and determine the Q (quality) factor of the peak.

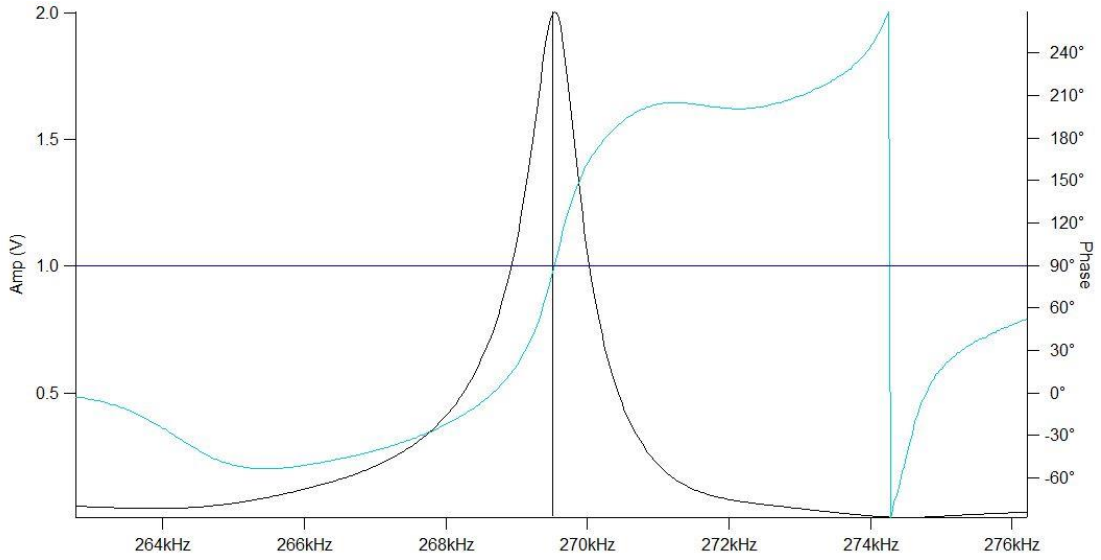

Figure 7. First resonant frequency of tune map

3.4.3 Elasticity calculate parameter

The experiment measures both morphology and mechanical properties of bone. As a result, the elasticity needs to be calibrated using a sample with known modulus. The sample I used in this research is silica, which has 72 GPa Young's modulus. Here are the steps to calibrate for getting Young's modulus.

1. Scan the silica sample using AMFM mode and get the young's modulus map of the scanning area.
2. Open the image scanned. Set the offline elasticity calculation to be the type

sphere and control the radius based on the Young's modulus simulated in offline calculation.

3. Copy the radius to "RealTime Elasticity Calc".

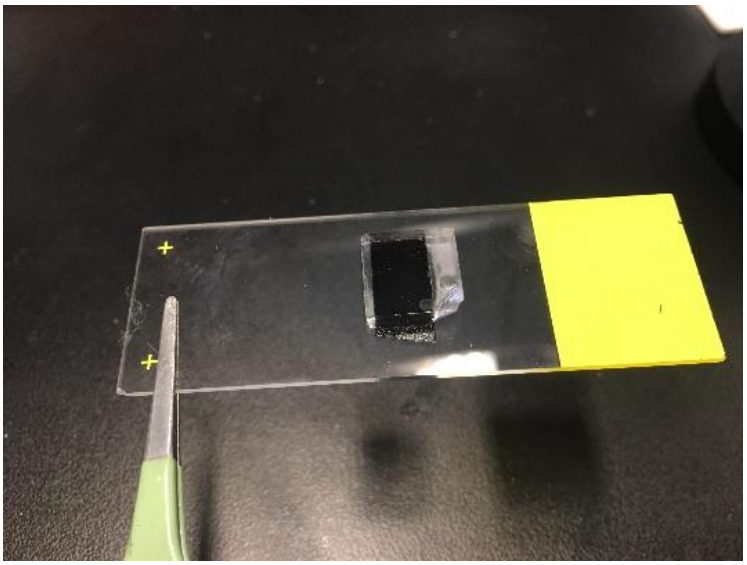

Figure 8. Silica Sample for finding tip radius

Chapter 4: Results and Discussion

As seen in the Figure 9, the optical microscopic image of the bone implant sample was obtained in which metal and bone matrix at the bone implant interface was clearly shown. Since the interfacial bone matrix adjacent metallic part undergoes active forming and remodeling after implantation to recover and fill the damaged area. Thus, the relatively newer bone matrix likely exists at the location closer to the metal implant. The red and blue boxes in Figure 9b indicate a newer and older bone region, respectively.

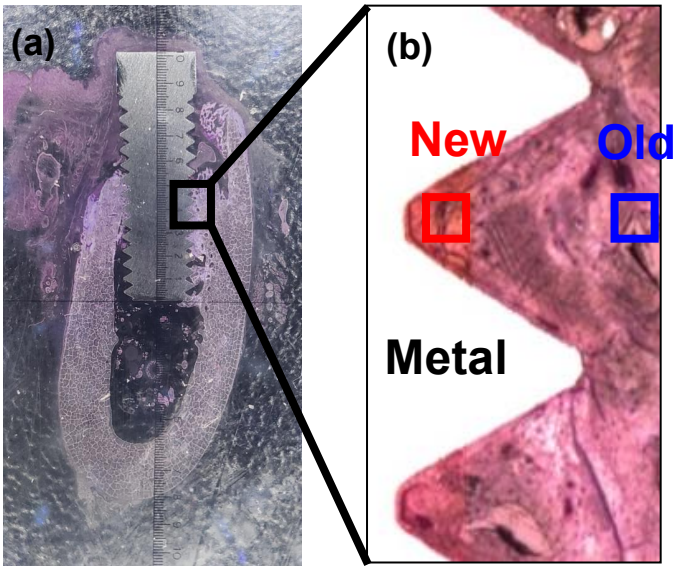

Figure 9. Optical microscopy image at the interface of the implant and bone matrix captured by 5x objective lens a), and 20x objective lens b). The red box represents the new bone area while the blue box represented the old bone area where bi-modal AFM

Here, bi-modal AFM was performed to investigate morphology and its mechanical property in the new and old bone region. The AFM result was shown in Figure 10. In each region, 4x4 μm^2 area was scanned, and topography and mechanical stiffness maps were obtained. Although the topographic map did not

show clear difference between new and old bone area, material composition and its orientation were clearly shown in the stiffness map. In the stiffness map, the brighter part means higher stiffness, while the dark area indicates lower stiffness. While the stiffness map of old bone revealed well-organized bone matrix, the map of new bone showed less organized pattern and seemed to be randomly orientated. Moreover, crystalline apatite structure and collagen fibrillar structure was clearly revealed in the old bone stiffness map. This result indicated that the matured bone matrix would have enough time to remodel its structure in response to mechanical input exerted in the region, which resulting in showing specific pattern of material composition. However, this result was not calibrated carefully, so the amplitude of stiffness map cannot be compared each other.

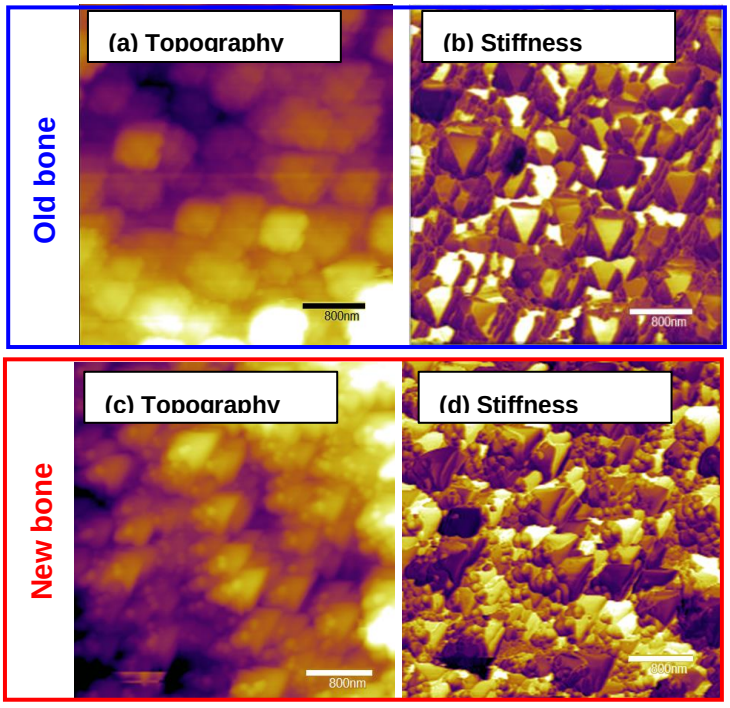

Figure 10. Nanoscale mapping of morphology and materials properties obtained by bi-modal AFM. (a), (b) shows topographic and mechanical information, respectively in old bone area. (c), (d) shows topographic and mechanical information in new bone area.

To overcome this, we followed calibration process discussed above part to obtain quantitative stiffness map to compare each area. By using calibrated bi-modal AFM, we investigated topography, surface texture, and young's modulus of new bone and old bone area. Here, 10x10 μm^2 area and 2x2 μm^2 area was examined in Figure 11 and 12, respectively for multi-scale characterization. In Figure 11, while the lower resolution morphology maps cannot distinguish the difference between the two area, the young's modulus was significant different between these two areas indicating young's modulus of old bone area was clearly higher than the modulus of new bone area. However, the difference in material composition in these two areas was not shown distinctly. The higher-resolution morphology maps in Figures 12 showed somewhat better discrimination in the morphological information, but it is not also easy to interpret how different they

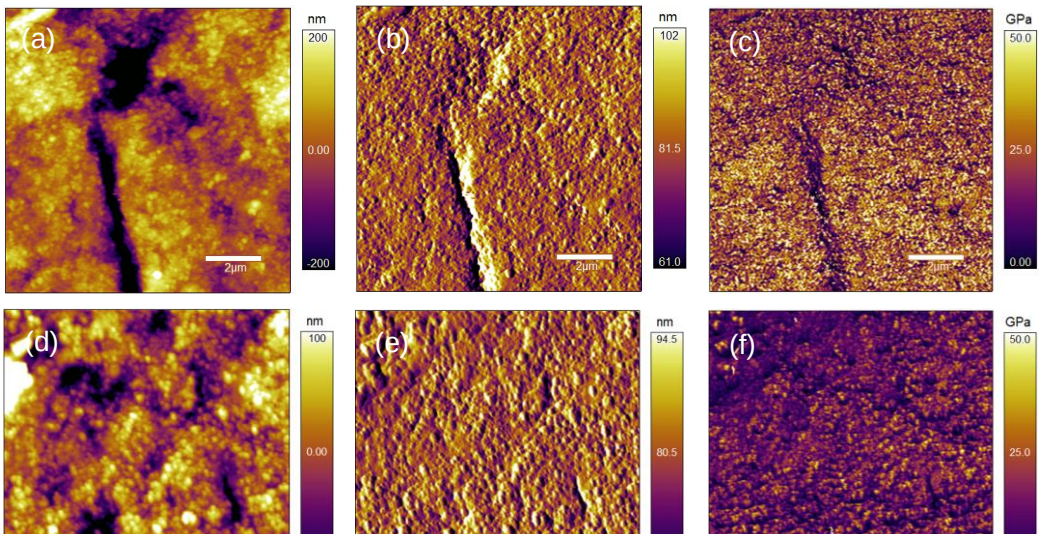

Figure 11. Morphology and stiffness maps of the bone in 10x10 μm^2 scale obtained by bi-modal AFM. (a), (d) shows topographic information of the sample in old bone and new bone area respectively. (b), (e) means surface texture of the sample, and (c), (f) are its stiffness map.

are except amplitude of young's modulus.

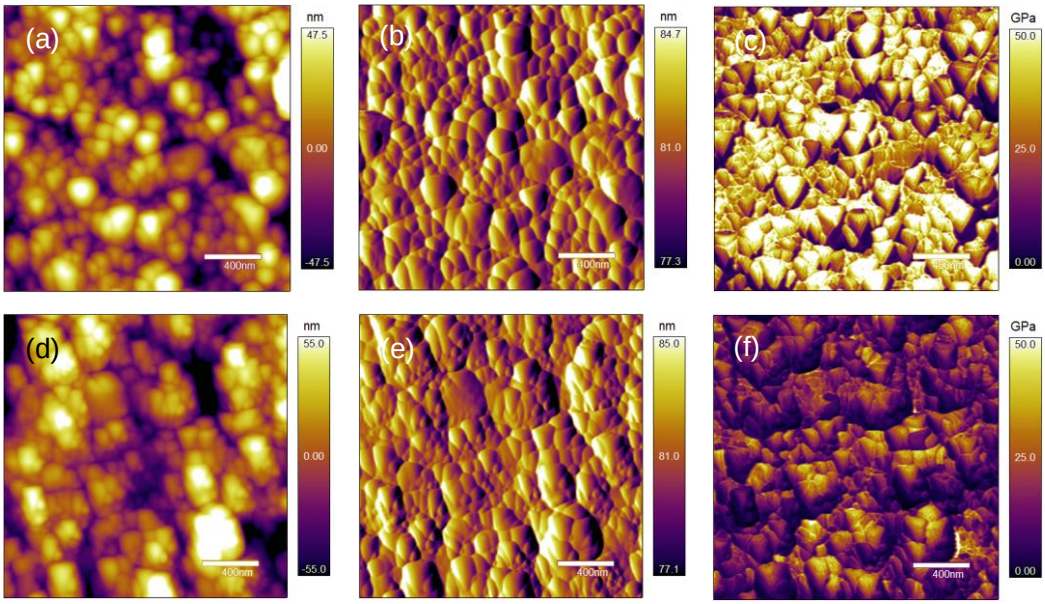

Figure 12. Morphology and stiffness maps of the bone in 2x2 μm^2 scale obtained by bi-modal AFM. (a), (d) shows topographic information of the sample in old bone and new bone area respectively. (b), (e) means surface texture of the sample, and (c), (f) are its stiffness map

For statistical analysis of the stiffness map between the new and old bone area, the young's modulus box plot was obtained as shown in Figure 13. Each box plot represented the mechanical property of new bone (red box) and old bone (blue box) area. The left two boxes indicate the young's modulus obtained in the 10x10μm^2 scanning area while the right two boxes show the modulus obtained in the 2x2 μm^2 scanning area. In each area, totally 65,536 young's modulus data point were examined. The box plot result indicated that young's modulus in lower resolution (10x10 μm^2) has lower average and deviation than it in higher resolution (2x2 μm^2), which indicated that young's modulus in higher resolution revealed more heterogeneous nature of the bone matrix. Moreover, mechanical property in new bone area was lower than it in the old bone area regardless of the scanning

size, which means that new bone area would not be fully matured yet and it would undergo mineralization process to increase its stiffness to reach the value in the case of old bone area.

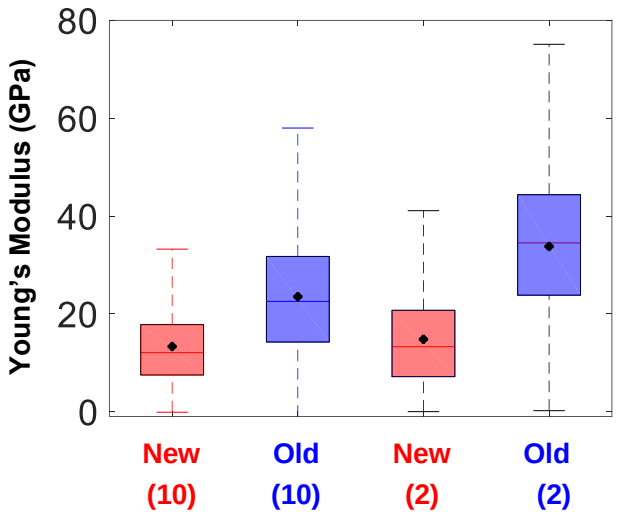

Figure 13. The boxplot representation of the mechanical property (Young's modulus) of new bone and old bone area obtained from 10x10 μm2, and 2x2 μm2 scanning area by bi-modal AFM respectively.

In addition, the histogram was obtained based on the young's modulus maps as shown in Figure 14. The histogram results indicated that the young's modulus in new bone was slanted toward left having most of them was located in a range of 0 to 20 GPa. In the other hand, the young's modulus of old bone was more evenly distributed ranging from 0 to 60 GPa than the case of new bone. Interestingly, even though the histogram of young' modulus in lower resolution seems to have one peak in new and old bone case, the histogram obtained in higher resolution clearly reveals two peaks in the old bone case. Considering that mineralized collagen has young's modulus less than 10 GPa and the bone mineral

has more than 20 GPa, each peak would represent collagen and mineral portion respectively in the area. This result also consisted with the box plot result, which reveals that the heterogeneity of material composition in the area cannot be fully represented in low resolution because it would not be enough to discriminate the collagen and mineral portion in the bone matrix.

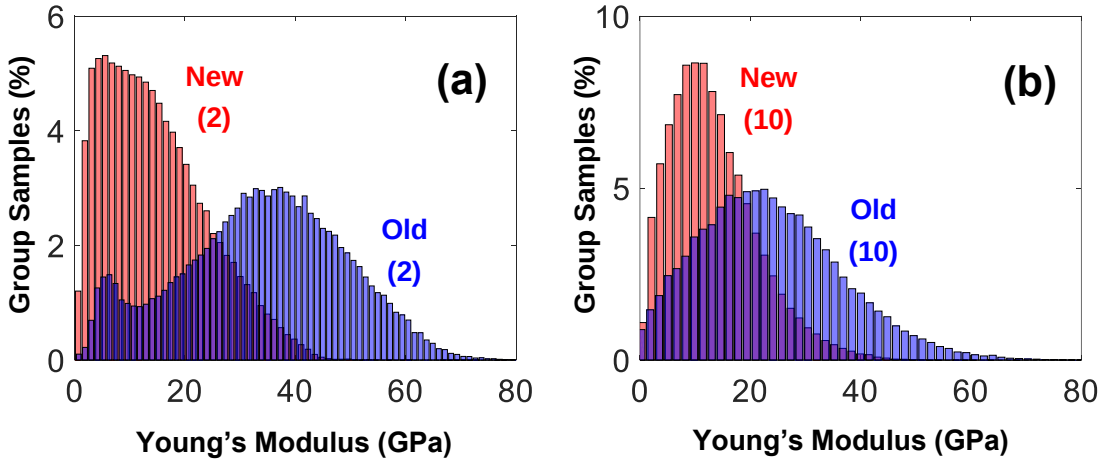

Figure 14. (a), (b) show the histogram representation of the Young's modulus from 10x10 μm^2, and 2x2 μm^2 scanning area by bi-modal AFM respectively.

Chapter 5: Conclusion

5.1 Summary

The morphology and mechanical property of bone matrix in a newly formed and pre-existing regions in a bone implant system were successfully investigated through an advanced bi-modal AFM technique. The current findings show the structural difference of bone matrix depending on the tissue age in which the arrangement of collagen fibril is ordered as the remodeling proceeds. In addition, the stiffness maps obtained by the bi-modal AFM techniques help to understand its mechanical structure in nanometer scale. In addition, the bi-modal AFM was carefully calibrated by using fused silica sample which has young's modulus of 72 GPa. Through the calibrated AFM, the quantitative young's modulus result was obtained and analyzed statistically based on box plot and its histogram, which reveals the heterogeneous nature of the bone matrix in high resolution.

5.2 Future work

In the future study, we will investigate gradual change of morphology and mechanical property following chronical change of bone matrix. Moreover, other advanced technique such as Fourier-Transform Infrared spectroscopy will be used to examine chemical composition in the area. These results would provide a better understanding of heterogeneous nature of the bone matrix

References

[1] Fratzl, P. and Gupta, H. S. and Paschalis, E. P. and Roschger, P. "Structure and mechanical quality of the collagen–mineral nano-composite in bone" J. Mater. Chem., 2004,14, 2115-2123 https://pubs.rsc.org/en/content/articlepdf/2004/jm/b402005g

[2] Matthew A Rubin, Iwona Jasiuk, Jeannette Taylor, Janet Rubin, Timothy Gany. "TEM analysis of the nanostructure of normal and osteoporotic human trabecular bone" Bone, Volume 33, Issue 3, 2003, 270-282

[3] Natalie Reznikov, Ron Shahar, Steve Weiner, "Bone hierarchical structure in three dimensions" Acta Biomaterialia, Volume 10, Issue 9, 2014, 3815-3826

[4] Hadjidakis, Dimitrios & Androulakis, Ioannis. "Bone Remodeling". Annals of the New York Academy of Sciences. 2007. 10. 385-96

[5] FROST, H.M. "Skeletal structural adaptations to mechanical usage (SATMU): 2. Redefining Wolff's law: the remodeling problem". 1990. Anat. Rec. 226: 414–422

[6] PETRTYL, M., J. HERT & P. FIALA."Spatial organization of the haversian bone in man". 1996. J. Biomech. 29: 161–169.

[7] PARFITT, A.M. "Osteonal and hemi-osteonal remodeling: the spatial and temporal framework for signal traffic in adult human bone". J. Cell Biochem. 1994. 55: 273–286.

[8] The SPM Application Guid (Version 13), AsylumResearch Oxford Instrument company, 2013.

[9] Hoffler, C. E., Guo, X. E., Zysset, P. K., and Goldstein, S. A."An Application of Nanoindentation Technique to Measure Bone Tissue Lamellae Properties." ASME. J Biomech Eng. 2005. 7. 1046–1053.

[10] Doerner, M. F., and Nix, W. D. "A Method for Interpreting the Data from Depth-sensing Indentation Instruments," J. Mater. Res.1986 .4. 601– 609.

[11] Zysset, P. K., et al. "Elastic Modulus and Hardness of Human Cortical and Trabecular Lamellae Measured by Nanoindentation," J. Biomech. 1999, 3210, 1005–1012.

[12] Yan Liu, Dan Luo, Tie Wang. "Hierarchical Structures of Bone and Bioinspired Bone Tissue Engineering". Special Issue: Advances in Nanobiotechnology. 2019. 12. 4611-4632